**Wind and Structures**, *Vol. 20, No. 1 (2015) 59-74*
DOI: http://dx.doi.org/10.12989/was.2015.20.1.059 

# Refined numerical simulation in wind resource assessment

Xue-Ling Cheng[1], Jun Li[1], Fei Hu[*1], Jingjing Xu[2] and Rong Zhu[3]

[1]*State Key Laboratory of Atmospheric Boundary Layer Physics and Atmospheric Chemistry, Institute of Atmospheric Physics, Chinese Academy of Sciences, Beijing 100029, P.R. China*
[2]*International Center for Climate and Environment Sciences, Institute of Atmospheric Physics, Chinese Academy of Sciences, Beijing 100029, P.R. China*
[3]*Public Weather Service Center China Meteorological Administration, Beijing 100081, P.R. China*

*(Received July 8, 2014, Revised October 9, 2014, Accepted November 27, 2014)*

**Abstract.** A coupled model system for Wind Resource Assessment (WRA) was studied. Using a mesoscale meteorological model, the Weather Research and Forecasting (WRF) model, global-scale data were downscaled to the inner nested grid scale (typically a few kilometers), and then through the coupling Computational Fluid Dynamics (CFD) mode, FLUENT. High-resolution results (50 m in the horizontal direction; 10 m in the vertical direction below 150 m) of the wind speed distribution data and ultimately refined wind farm information, were obtained. The refined WRF/FLUENT system was then applied to assess the wind resource over complex terrain in the northern Poyang Lake region. The results showed that the approach is viable for the assessment of wind energy.

**Keywords:** wind resource assessment; complex terrain; refined numerical simulation; WRF; FLUENT

## 1. Introduction

As coal, oil and other fossil fuel resources become depleted, research continues into finding a suitable replacement energy source. The main forms of renewable energy available are solar, wind and hydro. China enjoys abundant wind resources with substantial development potential. From 2007 to 2011, a fourth detailed national survey was completed and revealed the potential for wind resource development to be between 2000 and 3400 GW (Wang *et al*. 2011). As the wind power industry develops, improvements in the quality of the development of wind power are needed, such as wind resource assessment (WRA) techniques.

The main purpose of wind flow modeling is to estimate the wind resource at every proposed or potential wind turbine location so that the wind turbine's overall production can be calculated and its design can be optimized. This usually means extrapolating from the wind resource measured at one or more meteorological towers using a numerical wind flow model of some kind (Brower *et al*. 2010).

Since 2003, mesoscale numerical weather prediction (NWP) models have increasingly been used for regional wind mapping; nonlinear microscale models based on CFD are being developed and commercialized (Landberg *et al*. 2003, Rodrigo 2010). For instance, WindSim, developed in

*Corresponding author, Dr., E-mail: hufei@mail.iap.ac.cn


http://www.techno-press.org/?journal=was&subpage=8 ISSN: 1226-6116 (Print), 1598-6225 (Online)

Norway, is based on CFD methodology and is more suitable for rugged terrain than WAsP (Cattin *et al*. 2006). Other notable WRA models include WindPro (Thogersen *et al*. 2003, Ozerdem and Turkeli 2005), WindFarmer (Wang *et al*. 2006), and Meteodyn WT (Boquet 2010).

From the Chinese perspective, the China Meteorological Administration (CMA) has been contributing to the production of a wind atlas of China by developing wind resource numerical models that achieve a horizontal resolution of 5×5 km (Zhang *et al*. 2008), based on the Canadian wind energy simulation toolkit (WEST). In 2011, the Risø National Laboratory installed 11 sets of wind speed anemometers on the island of Bolund to obtain highly accurate wind speed data, and invited various research units to simulate the flow field with 57 CFD models for comparison purposes (Berg *et al*. 2011, Bechmann *et al*. 2011). The result calculated by CFD using the Reynolds Averaged Navier–Stokes (RANS) equation with a turbulence model was found to be the best.

Compared with mesoscale models, CFD can achieve wind simulation results with a much higher spatial resolution. The numerical schemes of most CFD tools are based on the finite volume method (FVM), which can be used in a grid system to fit the complex geometry. Many simulations of flow over realistic terrain with CFD tools have already been carried out and reported in the literature (Montavon 1998, Uchida and Ohya 1999, 2003, Stangroom 2004, Li and Chan 2012, Li *et al*. 2013).

Second, CFD models usually use simple wind profiles, such as a vertical logarithm wind profile, as the lateral boundary conditions, which cannot correctly describe the effects of the realistic terrain in the upwind direction. In the present study, we used a coupled model system involving a meteorological model, WRF (Weather Research and Forecasting model), and a commercial CFD model, FLUENT, to perform fine-scale wind simulations over realistic complex terrain. In the system, WRF is able to obtain large-scale circulation information from global-scale datasets, such as the National Centers for Environmental Prediction (NCEP) reanalysis dataset, and downscale it through nested-grid techniques to an area covered by FLUENT at regular time intervals, which can ensure that the inlet flow contains information on the realistic terrain in the upwind direction.

So, for the fine-scale simulation of the wind field over complex terrain, the most notable advantage of the WRF/FLUENT system is that WRF can provide realistic boundary conditions containing terrain information in the upwind direction and FLUENT can provide simulation results with a much higher spatial resolution and accurately represent complex terrain.

## 2. Refined numerical simulation method (WRF/FLUENT) over complex terrain

An approach based on off-line one-way nesting between a meteorological model, WRF, and a commercial CFD model, FLUENT, was applied to perform fine-scale wind simulations over real complex terrain (Fig. 1). More detailed procedures for the system are provided later in the paper through the example settings in the WRA of Poyang Lake.

First, we used the WRF model with three grid nests (54 km, 18 km and 6 km) to obtain large-scale circulation information from NCEP reanalysis data, and downscale it to the region for FLUENT (Fig. 2). Numbers of grid points were 68×68, 91×91 and 82×64 in the horizontal directions. The number of vertical layers was 32, with 12 layers under 1000 m, while sigma were 1, 0.998, 0.996, 0.994, 0.992, 0.989, 0.983, 0.970, 0.954, 0.934, 0.909 and 0.880. The range of the outer region was more than 3600 km, and the sigma was 0.87 at 1000 m and 0.842 at 1500 m. The physics options of the WRF model are listed in Table 1.

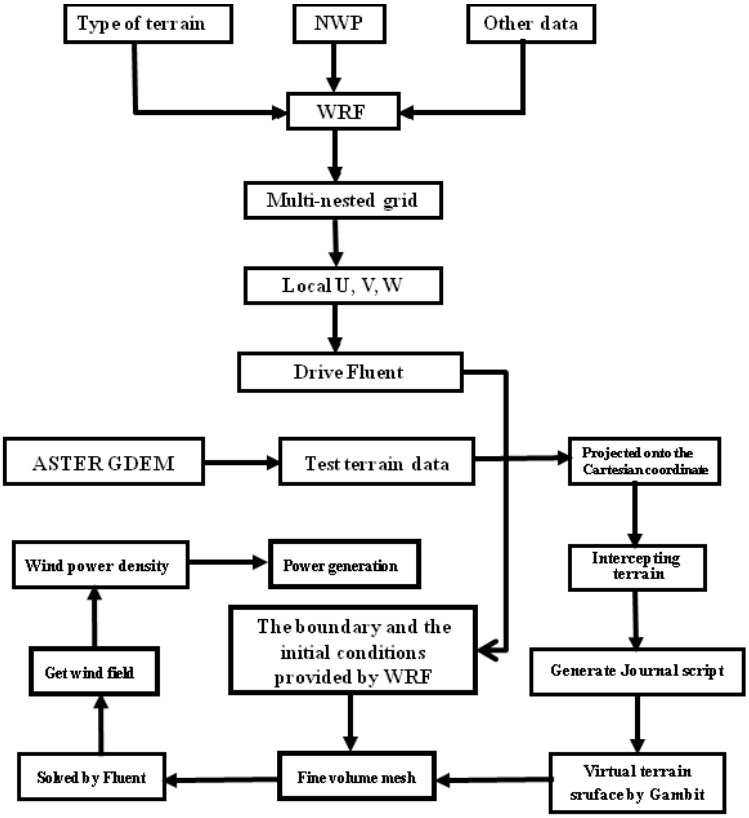


Fig. 1 The WRF/Fluent modeling system

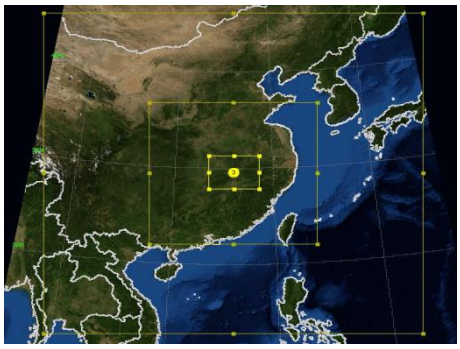

Fig. 2 WRF grids

Table 1 The physics options of the WRF model

| | |
|---|---|
| Microphysics | Lin scheme |
| Surface layer | Monin-Obukhov (Janjic Eta) Scheme |
| Land surface | Unified Noah land-surface model |
| Planetary boundary layer | YSU scheme |
| Longwave radiation | Rrtm scheme |
| Shortwave radiation | Goddard short scheme |
| Urban surface | No |
| Cumulus parameterization | Kain-Fritsch scheme (not adopted on third and forth layers) |
| Initialization | NCEP 1°×1° fnl data |
| Terrain | USGS 30″ data |

Next, before using FLUENT to simulate the wind field over complex terrain, it was necessary to input a Global Digital Elevation Model (GDEM) to set up the computation domain. One of the most complete collections of high resolution GDEM data is acquired by ASTER (the Advanced Spaceborne Thermal Emission and Reflection Radiometer). The ASTER GDEM is organized according to a regular grid of 30×30 m UTM-WGS84 cartographic coordinates, while the orthometric heights are determined using the corresponding ellipsoidal Earth Gravitational Model (EGM 96) geoid. It is free to download at http://www.csdb.cn/. Then, the ASTER GDEM database was converted into FLUENT grid. The boundary and initial conditions necessary for driving the FLUENT simulation runs were taken from the simulated results of WRF every hour.

The FLUENT simulation was performed in the RANS framework. The airflow was considered as incompressible and viscous. The Coriolis force was neglected because the characteristic scale of the simulation domain was in the order of kilometers. The turbulence closure model adopted in the FLUENT simulation was the realizable $k$-$\varepsilon$ model, which is the best one among all the $k$-$\varepsilon$ models integrated in FLUENT in light of the studies by Li *et al*. (2004, 2006).

## 3. Detailed investigation of wind energy resources in the Poyang Lake region of Jiangxi Province

The plain of Poyang Lake lies in the north of Jiangxi Province. Widespread low and hilly land is situated outside the area of the plain, and the ground is undulating (50–100 m above sea level). Inside the area of the plain is a polder area, with an elevation of below 20 m, and from Hukou to Jishan there exists a narrow 90 km lake road. In the south of the lake, the water surface is broad, and complex terrain exists around the lake. The north side is close to Lushan, and the east features the highest peak (Huanggang Hill) with an altitude of 2157 m (Fig. 3). In winter, cold high pressure system from Siberia and Mongolia control and influence the region, with northerly winds prevailing; while in the summer, the influence comes from the western Pacific subtropical high, with southerly winds prevailing. Through the interaction of terrain, valley winds and land–lake

breezes, there is a complex structure to the atmospheric boundary layer, local climate, and the distribution of wind resources. In the region of the lake road, owing to the stability of the wind direction and high-quality wind resources, multiple anemometer towers have been built; namely, Shizishan Tower, Zaohu Tower, Laoyemiao Tower, Shaling Tower, Rocky Hill Tower, and Jishan Tower (see Table 2 for detailed information about the towers).

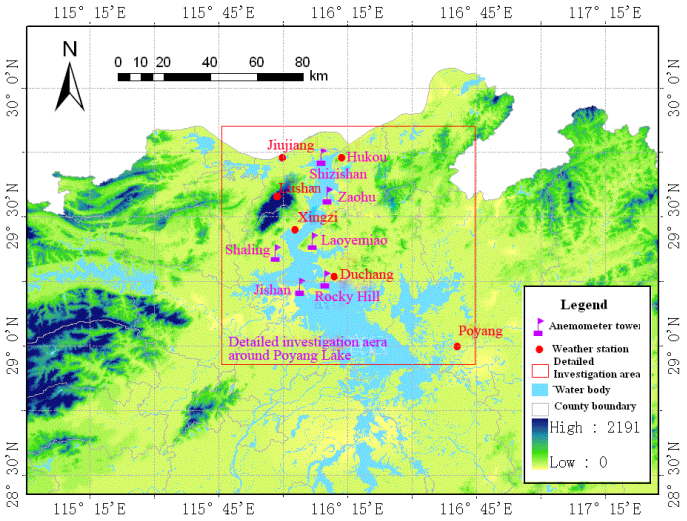


Fig. 3 Terrain around Poyang Lake

Table 2 The anemometer towers around Poyang Lake

| Number | Site | Name | Latitude | Longitude | Elevation(m) | Terrain | Area ($km^2$) | Height (m) | Levels |
|---|---|---|---|---|---|---|---|---|---|
| 14001 | Lushan Region | Shizishan | 116:09:17.82 | 29:44:3.60 | 96 | low hilly land | 2.8 | 70 | 4 |
| 14002 | Duchang County | Rocky Hill | 116:10:12.76 | 29:15:37.00 | 87 | hill | 8.6 | 70 | 4 |
| 14004 | Young County | Jishan | 116:04:17.46 | 29:13:50.16 | 89 | low hilly land | 17.5 | 70 | 4 |
| 2973 | Xinzi County | Shaling | 29:22:48.12 | 116:01:9.54 | 48 | low hilly land | | 100 | 5 |
| 2943 | Hukou County | Zaohu | 29:35:51.54 | 116:12:6.84 | 20 | low hilly land | | 100 | 5 |
| 2619 | Duchang County | Laoyemiao | 29:24:59.52 | 116:06:5.1 | 156 | low hilly land | | 70 | 4 |

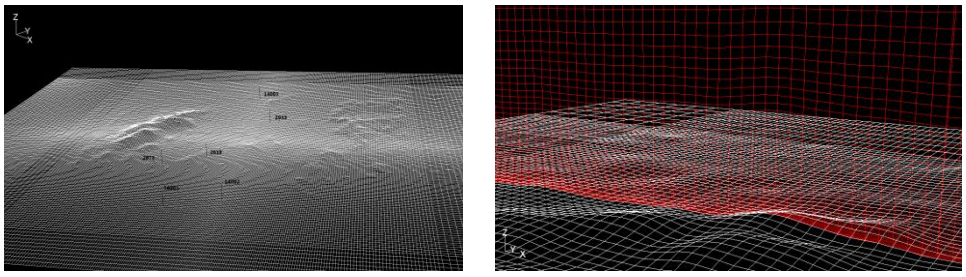

Fig. 4 Horizontal and vertical grids of the Poyang Lake region use by FLUENT

Our simulation results were first compared with the observation data of those towers, and were then used to analyze the wind resource of this region. During the following discussion, the towers are denoted by their numbers shown in Table 2. Fig. 4 shows the FLUENT grids (the lines are the anemometer towers) of the terrain of the Poyang Lake region. The fine grids have a horizontal resolution of 50 m and a vertical resolution of 10 m under a height of 150 m. The total area is 64×74 km. And the area of 6×6 km around each tower is used as the innermost domain for Fluent to calculate the wind field of them separately.

The simulation period was 2010-12-13 to 2011-12-31 (LST, same as below). The simulation results include the flow field over the six innermost domains every one hour, and the wind velocities at each level of the six towers at intervals of every 15 mins.

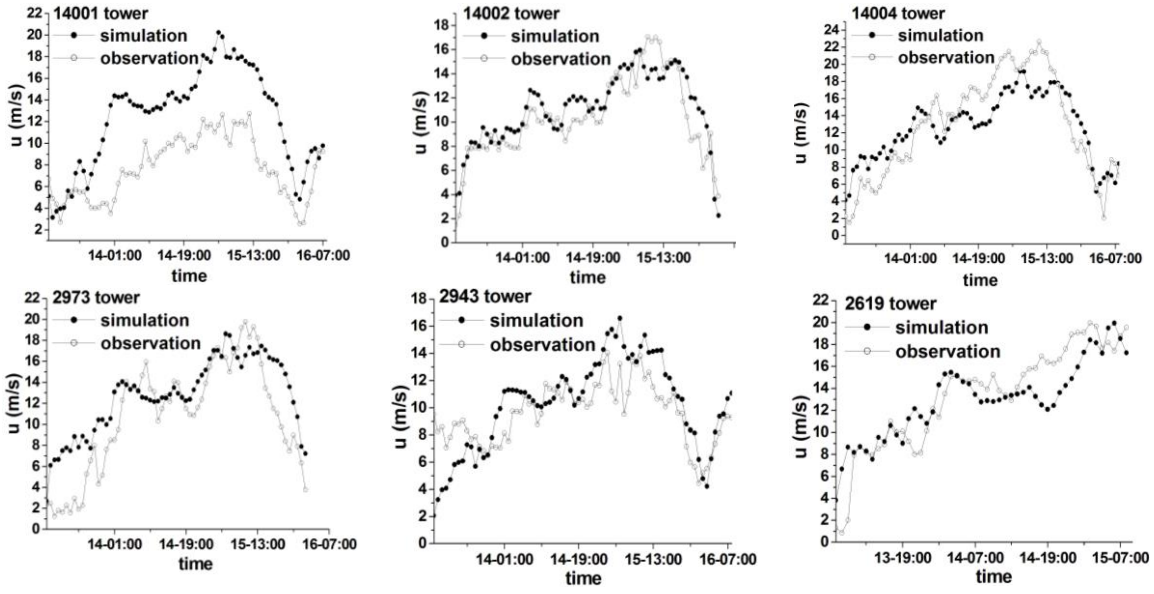


Fig. 5 Comparison of simulated and observed velocities from 2010-12-13 08:00 to 2010-12-16 08:00

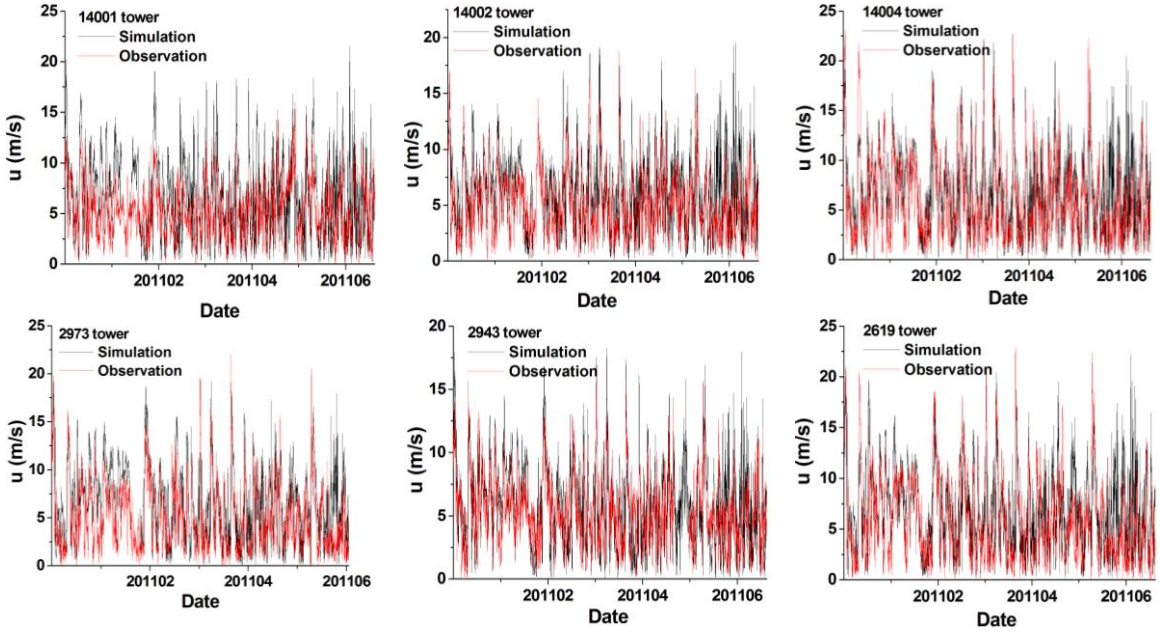


Fig. 6 Comparison of simulated and observed velocities from January to June 2011

First, we used the tower data to test the accuracy of the calculations. Because it is very difficult to simulate the wind velocity during transitioning weather, we chose a cold snap weather event on 2010-12-15 for the simulation. Fig. 5 shows a comparison of simulated and observed velocities at the turbine hub height (70 m) of the six towers from 2010-12-13 08:00 to 2010-12-16 08:00. The original simulation data are at intervals of 15 mins and the observation data are at intervals of 10 mins; here, we use hour-averaged data for comparison. From Fig. 5, we can see that the wind increasing during the cold snap was captured well by the simulation results.

Furthermore, Fig. 6 shows a comparison of the first half of 2011 at 70 m. As can be seen, the velocity changes of the simulations and observations are almost same. However, to analyze the simulation results in more depth, quantitative comparisons are needed.

We calculated three errors between simulated and observed results: the bias, root-mean-square error (RMSE), and relative error ($\varepsilon$) of wind velocities

$$\text{Bias} = \frac{\sum_{i=1}^{N}\left(X_i - Y_i\right)}{N} \tag{1}$$

$$\text{RMSE} = \sqrt{\frac{\sum_{i=1}^{N}\left(X_i - Y_i\right)^2}{N}} \tag{2}$$

$$\varepsilon = \frac{\sum_{i=1}^{N} |X_i - Y_i|}{\sum_{i=1}^{N} Y_i} \times 100\% \quad (3)$$

where $X_i$ and $Y_i$ are the simulated and observed velocities, respectively, and $N$ is the sample size.

The bias and RMSE during different times at 70 m are given in Table 3, and the relative errors for the six towers at 70 m are shown in Fig. 7. From the results, we can see that, during cold weather, the simulations of the six towers are different. The bias of tower 14004 is the smallest, while that of tower 14001 is the largest. This is perhaps because, during cold weather, a strong northwest wind blows along the narrow 90-km lake road from Hukou to Jishan; and given that tower 14001 is located at the beginning of the road, and tower 14004 is at the end of the road, during the simulation, the flow field of the latter develops fully, and so the simulation result is more accurate.

Furthermore, the biases of the six towers change in different months with almost same tendency, the bias in January is largest and the bias in May is smallest, most likely because transition weather in May occurs relatively less frequently than in January. We can see similar results based on the data in Fig. 7. Meanwhile, the RMSE changes very little, being between 1.6 and 4.2.

Table 3 The bias and RMSE during different times

| Time | Error (m/s) | 14001 | 14002 | 14004 | 2973 | 2943 | 2619 |
|---|---|---|---|---|---|---|---|
| **2010.12.13-16** | **Bias** | 4.6 | 0.7 | -0.2 | 2.0 | 0.6 | -0.3 |
| | **RMSE** | 2.7 | 1.6 | 3.0 | 2.7 | 2.2 | 2.4 |
| **2011.01** | **Bias** | 3.7 | 2.1 | 1.8 | 3.1 | 1.7 | 1.6 |
| | **RMSE** | 2.1 | 2.0 | 2.7 | 2.2 | 2.0 | 2.8 |
| **2011.02** | **Bias** | 1.2 | 0.7 | 0.5 | 1.6 | 0.2 | 0.1 |
| | **RMSE** | 3.6 | 3.0 | 3.5 | 3.2 | 2.8 | 3.6 |
| **2011.03** | **Bias** | 1.8 | 1.2 | 1.0 | 1.5 | 0.6 | 0.9 |
| | **RMSE** | 3.3 | 2.5 | 3.2 | 3.0 | 2.8 | 3.5 |
| **2011.04** | **Bias** | 1.0 | 1.1 | 0.8 | 1.0 | 0.3 | 1.0 |
| | **RMSE** | 3.6 | 3.3 | 3.7 | 3.6 | 2.8 | 3.9 |
| **2011.05** | **Bias** | 0.3 | 0.5 | 0.2 | 0.9 | -0.2 | 0.7 |
| | **RMSE** | 3.5 | 2.8 | 3.6 | 3.2 | 2.7 | 4.0 |
| **2011.06** | **Bias** | 1.2 | 2.1 | 2.2 | 2.9 | 1.0 | 2.6 |
| | **RMSE** | 4.2 | 3.8 | 4.2 | 3.6 | 3.4 | 4.2 |

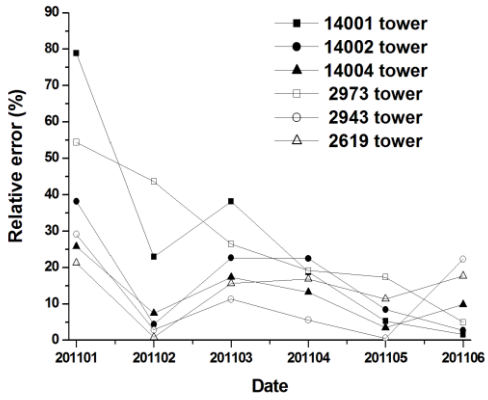


Fig. 7 Relative errors of monthly-averaged speeds of the six towers at 70 m height

Next, we used the coupled model system to calculate the distributions of wind resources around the Poyang Lake region. First, we calculated the wind direction and compared the simulation results with observation data. Fig. 8 shows the monthly averaged wind rose map of tower 2973 at 70m height in January, April and June. The simulation results agree with observation well, and the changes of wind direction in different season are obvious. In January, there was mainly northeast wind. The wind direction changed in April, there were both northeast wind and southwest wind. And in June, the wind direction was mainly southwest. Then, we calculated the wind distributions around the six innermost domains, and Figs. 9(a)-9(d) show the monthly-averaged wind distributions around the six tower regions in January, March, July, September. We can see that the wind resources in these regions are all very rich and change with the seasons. In these figures, the wind is at a height of 70 m above ground, and *y* represents north and *x* represents east. From the results, we can see that in winter (i.e., January), mainly northerly winds exist; in summer (i.e., July), southerly winds are dominant; in spring (i.e., March), the winds are mainly westerly; and in autumn (i.e., September), the main wind direction is easterly.

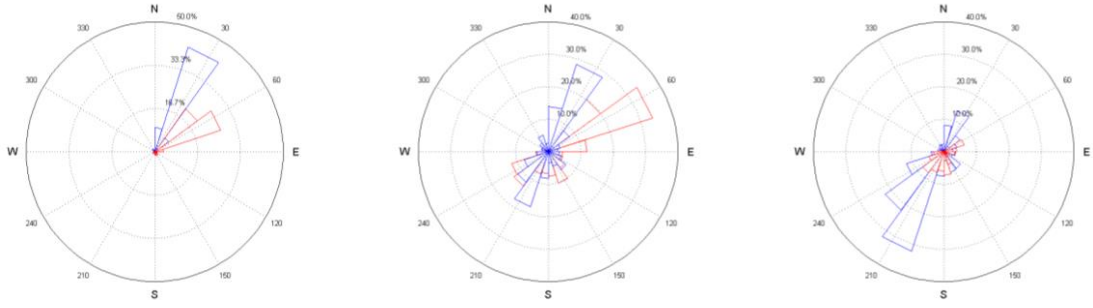


(a) (b) (c)

Fig. 8 Monthly averaged wind direction rose map at tower 2973 at 70 height by simulation (blue) and observation (red): (a) January, (b) April, (c) June

In January, when northerly winds are dominant, we can see that, because tower 14001 lies in the north, at the beginning of the narrow north–south-oriented 90-km lake road, the winds are largest in this area. In March, westerly winds are dominant, but the wind velocity is weaker than in January. July features southerly winds. In September, the wind velocities are weaker than over the whole year; while January is the only month to feature wind velocities greater than those over the whole year.

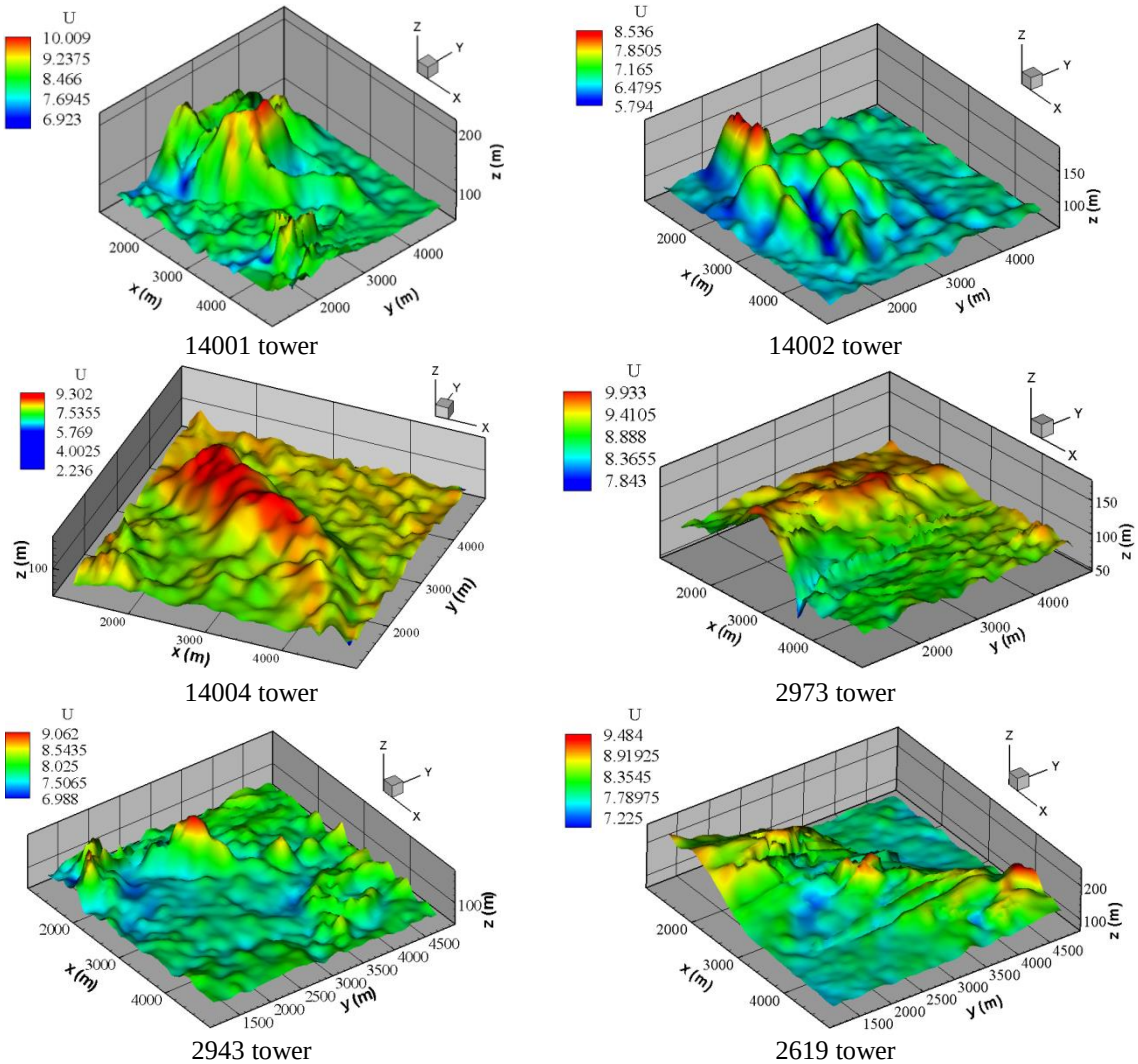


Fig. 9(a) Wind distributions in January

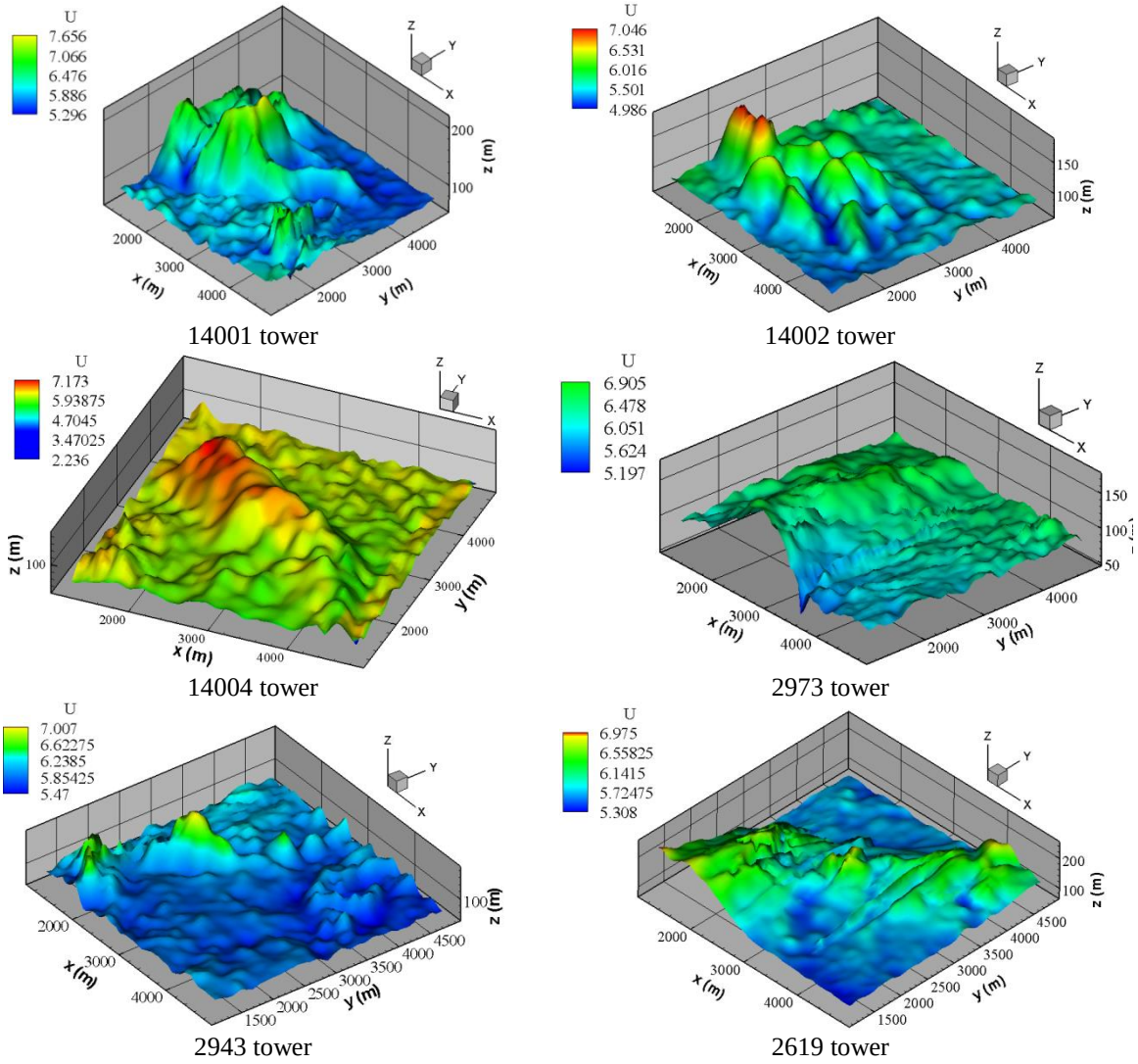


Fig. 9(b) Wind distributions in March

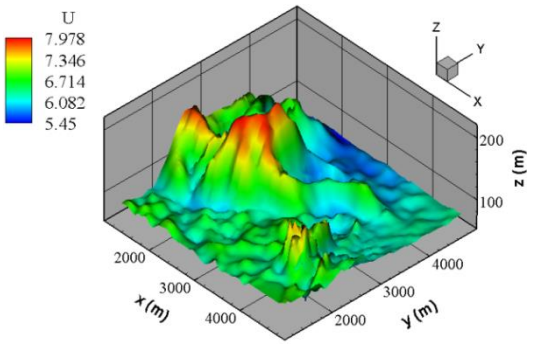


14001 tower

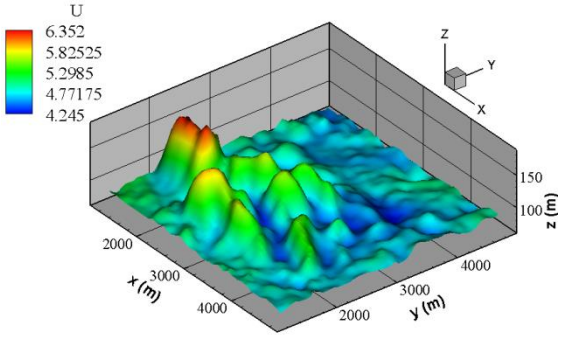


14002 tower

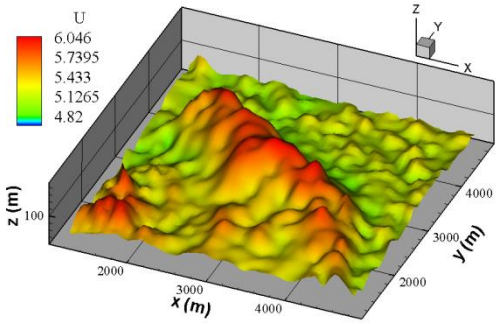


14004 tower

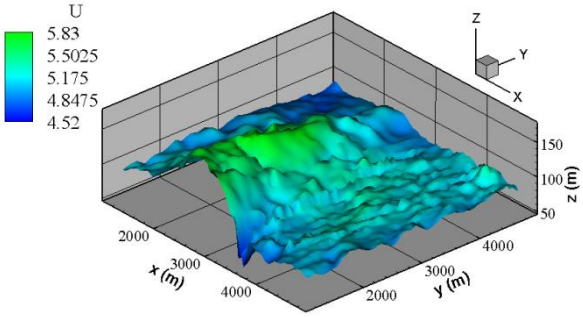


2973 tower

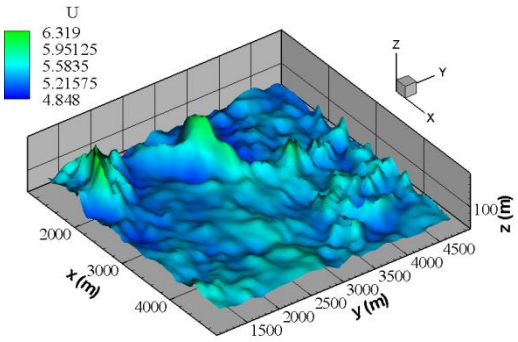


2943 tower

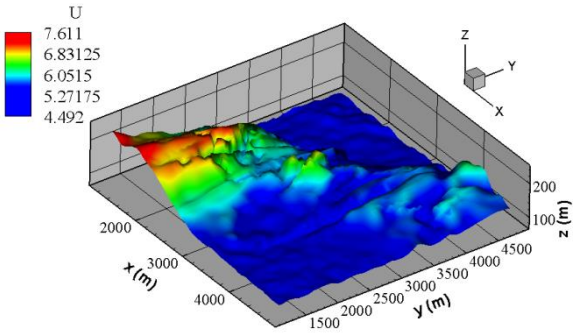


2619 tower

Fig. 9(c) Wind distributions in July

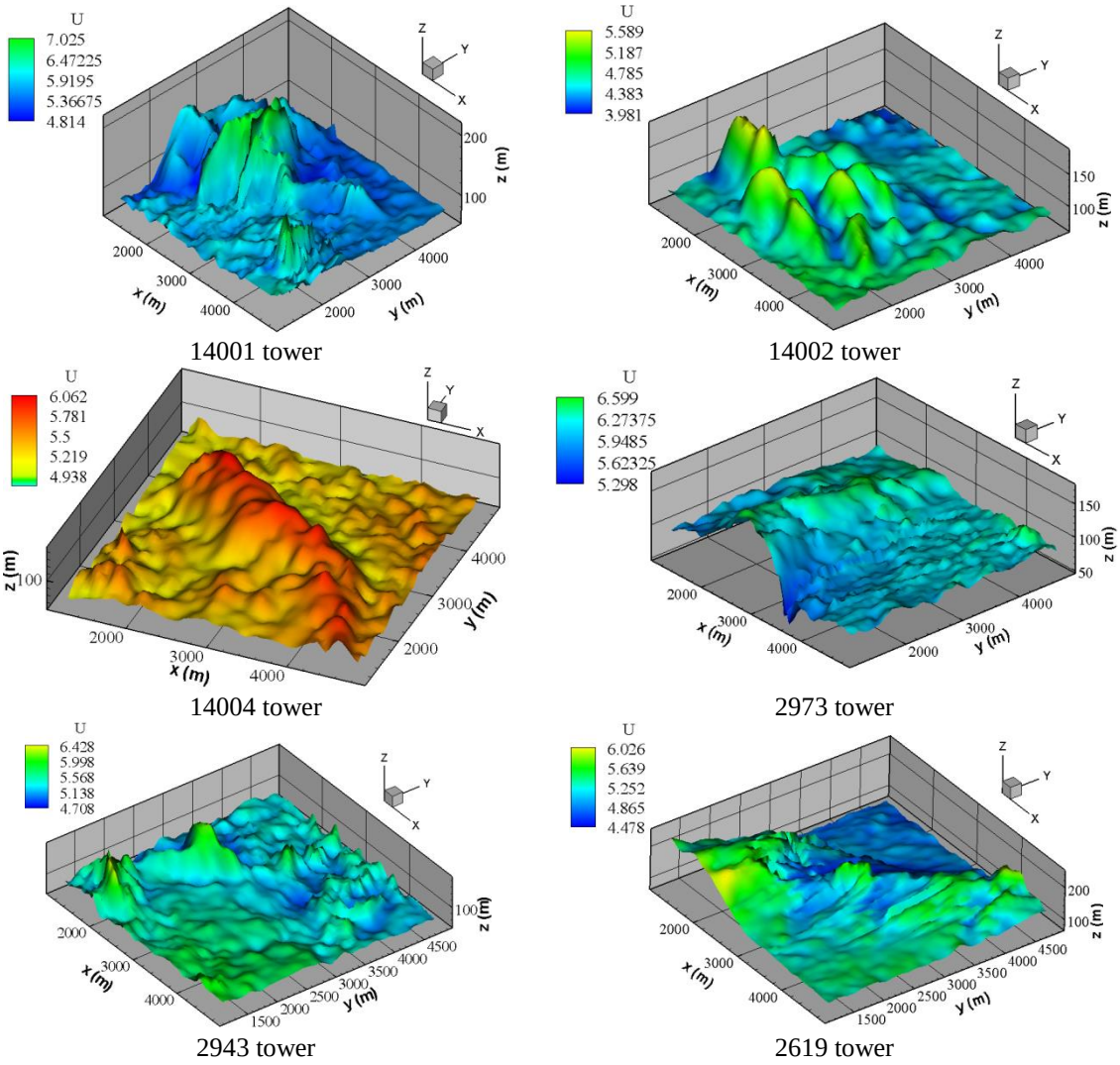


Fig. 9(d) Wind distributions in September

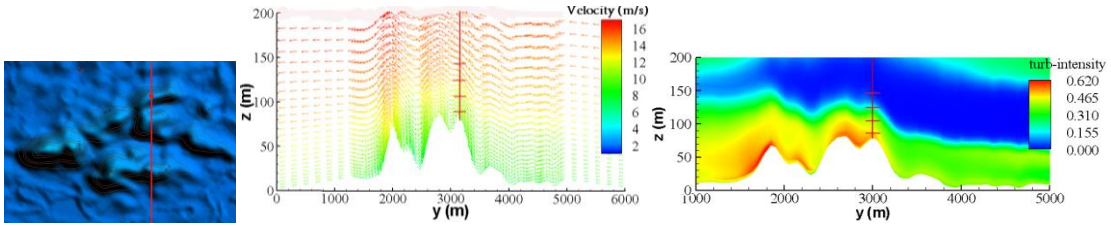


Fig. 10 Vertical profiles of velocity and turbulence intensity of a south–north cross section passing through tower 14002

For a detailed investigation of the wind resource around each tower, the vertical profiles of wind vector and turbulence intensity are shown in Fig. 10. In the following, we analyze the wind around tower 14002 at 08:00 December 15, 2010 as an example.

Fig. 10 shows a south–north cross section passing through tower 14002. In the left-hand panel, the red line shows the position of the section, while the dot is the position of the tower. In the middle and right-hand panels, are the vertical profiles of wind velocity vector and turbulence intensity through the section, and the red line on the hill is the tower, and the four horizontal lines across the tower are the anemometers at heights of 10 m, 30 m, 50 m and 70 m. From the bottom to the top, the velocities recorded by the anemometers were 11 m/s, 12.1 m/s, 13.8 m/s and 14.5 m/s, demonstrating that the velocity increased with an increase in height. The turbulence intensities, from bottom to top, were 45.5%, 36.8%, 8.43% and 0.98%, showing a decrease with height, and were larger on the windward slope than on the downwind slope.

From these analyses, we can basically determine the distributions of wind resource around the Poyang Lake region. In this area, the wind resource is rich throughout the year, but especially in winter. Related to this, the winds are strongest in the region around tower 14001, which is a very suitable area for building a wind farm. Because it lies in the north of the narrow lake road, during winter, there is mainly northerly wind, at the beginning of the lake road, for the effect of narrow, the wind is strong, and around the tower, the wind resource is rich. Furthermore, the wind is stronger at the top of the hill, rather than at the bottom; so, if possible, the turbines should be located at higher elevations. However, the turbulence intensities are greater on the windward slope than the downwind slope, and this should be considered for turbine sitting.

In this paper, the WRF/FLUENT system based on off-line one-way nesting was applied to perform fine-scale wind simulations over real complex terrain. Now, this system is only one-way coupled. To improve the simulation accuracy, the two-way coupled method should be considered in the future.

## 4. Conclusions

An approach based on offline one-way nesting between a meteorological model, WRF, and a commercial CFD model, FLUENT, was applied to perform fine-scale wind simulations over realistic complex terrain. A data interface was designed, and then the boundary and initial conditions necessary for driving the FLUENT simulation runs were taken from the simulated results of the WRF model at regular time intervals, ensuring that the boundary conditions for the

FLUENT simulations were more realistic. Using the WRF/FLUENT system, a WRA of the Poyang Lake region was produced. The system was able to provide a detailed distribution of wind resources, and at a better resolution than WRF

## Acknowledgements

This work was supported by the Direction Program of the Institute of Atmospheric Physics: "The research and application demonstration of a wind power short-term forecasting model system on a large wind farm" (Y267014601), the National Development and Reform Commission and Ministry of Finance of the People′s Republic of China grant: "Detailed Wind Energy Resource Assessment of China", the laboratory open project of China Electric Power Research Institute "Refined Numerical Simulation of wind farm base on CFD downscaling method" and the National Natural Science Foundation of China (41375018).

### References

Bechmann, A., Sørensen, N.N., Berg, J., Mann, J. and Réthoré, P.E. (2011), "The Bolund experiment, part II: blind comparison of microscale flow models", *Bound. - Lay. Meteorol.*, **141**(2), 245-271.

Berg, J., Mann, J., Bechmann, A., Courtney, M. and Jørgensen, H. (2011), "The Bolund experiment, part I: flow over a steep, three-dimensional hill", *Bound. - Lay. Meteorol.*, **141**(2), 219-243.

Boquet, M. (2010), "Innovative solutions for pulsed wind LiDAR accuracy in complex terrain", *Proceedings of the 15th International Symposium for the Advancement of Boundary Layer Remote Sensing*, Paris.

Brower, M., Marcus, M., Taylor, M. *et al*. (2010), *Wind Resource Assessment Handbook*, New York State Energy Research and Development Authority, AWS Truepower, 203pp.

Cattin, R., Schaffner, B. and Kunz, S. (2006), "Validation of CFD wind resource modeling in highly complex terrain", *Proceedings of the Fourth European Wind Energy Conference*, Athens, Greece, European Wind Energy Association.

Landberg, L., Myllerup, L., Rathmann, O., Petersen, E.L., Jørgensen, B.H., Badger, J. and Mortensen, G. (2003), "Wind resource estimation – an overview", *Wind Eng.*, **6**(3), 261-271.

Li, L., Hu, F., Cheng, X.L. and Han, H.Y. (2004), "The application of computational fluid dynamics to pedestrian level wind safety problem induced by high-rise buildings", *Chinese Phys.*, **13**(7), 1070-1075.

Li, L., Hu, F., Cheng, X.L., Jiang, J.H. and Ma, X.G. (2006), "Numerical simulation of the flow within and over an intersection model with Reynolds-averaged Navier-Stokes method", *Chinese Phys.*, **15**(1), 149-155.

Li, L., Chan, P.W. (2012), "Numerical simulation study of the effect of buildings and complex terrain on the low-level winds at an airport in typhoon situation", *Meteorologische Zeitschrift*, **21**(2), 183-192.

Li, L., Chan, P.W., Zhang, L.J. and Hu, F. (2013), "Numerical simulation of a lee wave case over three-dimensional mountainous terrain under strong wind condition", *Adv. Meteorol.* **2013**, Article ID 304321.

Montavon, C. (1998), "Validation of a non-hydrostatic numerical model to simulate stratified wind fields over complex topography", *J. Wind Eng. Ind. Aerod.*, **74-76**, 273-282.

Ozerdem, B., Turkeli, H.M. (2005), "Wind energy potential estimation and micrositting on Izmir Institute of Technology Campus, Turkey", *Renew. Energ.*, **30**(10), 1623-1633.

Rodrigo, J.S. (2010), *State-of-the-Art of Wind Resource Assessment*. Wind Resource Assessment Audit and Standardization Project.

Stangroom, P. (2004), *CFD Modelling of Wind Flow over Terrain*, PhD Thesis, University of Nottingham, 298pp.

Thogersen, M.L., Nielsen, P., Mads, V.S. *et al*. (2003), "Applying new computer-aided tools for wind farm planning and environmental impact analysis", *Proceedings of the 2003 European Wind Energy Conference & Exhibition*, CD 2, Madrid, Spain.

Uchida, T. and Ohya Y. (1999), "Numerical simulation of atmospheric flow over complex terrain", *J. Wind Eng. Ind. Aerod.*, **81**, 283-293.

Uchida, T. and Ohya Y. (2003), "Large-eddy simulation of turbulent airflow over complex terrain", *J. Wind Eng. Ind. Aerod.*, **91**(1-2), 219-229.

Wang, Y., Smith, G.M. and Schlez, W. (2006), "Recent developments in precision wind farm modeling", *Proceedings of the Asian Wind Energy Conference & Exhibition*, 20060628-30, Beijing(CN).

Wang, Z.Y., Shi, J.L., Zhao, Y.Q. *et al*. (2011), *China Wind Energy Development Roadmap 2050*, Energy Research Institute, National Development and Reform Commission (NDRC) of P. R. China.

Zhang, D., Zhu, R., Luo, Y. *et al*. (2008), "Application of wind energy simulation toolkit (WEST) to wind energy numerical simulation of China", *Plateau Meteorology*, **27**(1), 202-207.

*CC*